

Prominence activation, optical flare, and post-flare loops on the RS Canum Venaticorum star SZ Piscium

Dongtao Cao,^{1,2*} Shenghong Gu,^{1,2,3†} Jian Ge,⁴ Tinggui Wang,⁵ Jilin Zhou,⁶ Liang Chang,^{1,2} U. Wolter,⁷ M. Mittag,⁷ J. H. M. M. Schmitt,⁷ and V. Perdelwitz⁷

¹Yunnan Observatories, Chinese Academy of Sciences, Kunming 650216, China

²Key Laboratory for the Structure and Evolution of Celestial Objects, Chinese Academy of Sciences, Kunming 650216, China

³University of Chinese Academy of Sciences, Beijing 100049, China

⁴Department of Astronomy, University of Florida, Bryant Space Science Center, Gainesville, Florida 32611, USA

⁵Key Laboratory for Research in Galaxies and Cosmology, Department of Astronomy, University of Science and Technology of China, Chinese Academy of Sciences, Hefei 230026, China

⁶Department of Astronomy and Key Laboratory of Modern Astronomy and Astrophysics in Ministry of Education, Nanjing University, Nanjing 210093, China

⁷Hamburger Sternwarte, Universität Hamburg, Hamburg 21029, Germany

Accepted 2018 October 10. Received 2018 October 9; in original form 2018 June 6

ABSTRACT

We present the results of time-resolved high-resolution spectroscopic observations of the very active RS Canum Venaticorum (RS CVn) star SZ Piscium (SZ Psc), obtained during two consecutive observing nights on October 24 and 25, 2011. Several optical chromospheric activity indicators are analyzed using the spectral subtraction technique, which show the remarkably different behavior between two nights. Gradually blue-shifted and strengthened excess absorption features presented in the series of the subtracted spectra (especially for the H α , He I D₃ and H β lines), as a result of active stellar prominence that is rising its height along the line of our sight, was detected in the observations on October 24. This prominence activation event was probably associated with the subsequently occurred optical flare, and part of that flare decay phase was hunted in the observations on October 25. The flare was characterized by the prominent He I D₃ line emission, as well as stronger chromospheric emission in the H α , H β and other active lines. The gradual decay of flare was accompanied by an obviously developmental absorption feature in the blue wing of the H α and other active lines, which could be explained as cool post-flare loops which projected against the bright flare background. Therefore, a series of possibly associated magnetic activity phenomena, including flare-related prominence activation, optical flare and post-flare loops, were detected during our observations.

Key words: stars: activity — binaries: spectroscopic — stars: chromospheres — stars: flare — circumstellar matter – stars: individual: SZ Psc

1 INTRODUCTION

Solar-type activity phenomena including starspots, plages, flares and prominences, have been widely observed in many cool stars (Schrijver & Zwaan 2000). It is commonly assumed that all of these active phenomena arise from a powerful magnetic dynamo generated by the interplay between the turbulent motions in the convection zone and the stellar differential rotation, in a manner similar to the Sun. Therefore, the solar activity paradigm provides a good

reference to investigate magnetic activity phenomena encountered in solar-like stars. To detect stellar prominences and capture the other related transient activity events, in our present work, we performed time-resolved spectroscopic observations for SZ Psc.

The star SZ Psc (HD 219113, SAO 128041) is a well known double-lined spectroscopic and partial eclipsing binary system with an orbital period of about 3.97 days. The system consists of a more massive K1 IV primary component which fills 80–90% of its Roche lobe and a F8 V secondary companion (Jakate et al. 1976). Based on the star’s changing systemic velocity, Eaton & Henry (2007) argued that there is a tertiary component in the system.

* E-mail: dtcao@ynao.ac.cn

† E-mail: shenghonggu@ynao.ac.cn

Furthermore, applying the least squares deconvolution (LSD) method, Glazunova et al. (2008) detected the signature of the tertiary component appears in the mean line profile of SZ Psc. More recently, using the similar method, Xiang et al. (2016) have also confirmed the existence of the tertiary star in the SZ Psc system and obtained its mass and orbital period of about $0.9 M_{\odot}$ and 1283 ± 10 days, respectively. The contribution of the tertiary star to the luminosity of the system was also estimated to be about 5%, which is in good agreement with the contribution of about 3–4% derived by Eaton & Henry (2007).

SZ Psc belongs to the RS CVn class of variable stars (Hall 1976; Fekel, Moffett, & Henry 1986), which are characterized by particularly intense magnetic activity that manifests itself in the form of remarkable photometric variability caused by changing spot coverage, chromospheric activity, transition region and coronal emission. The starspot activity on SZ Psc has been studied through photometry by several authors (e.g. Eaton & Hall 1979; Lanza et al. 2001; Kang et al. 2003; Eaton & Henry 2007). The long-term starspot evolution, a possible activity cycle, and orbital period variation have been investigated by Lanza et al. (2001), based on an extended sequence of light curves obtained between 1957 and 1998. The first Doppler images of SZ Psc derived by Xiang et al. (2016) show that the K1 IV star exhibits pronounced high-latitude spots as well as numerous intermediate- and low-latitude spot groups during the entire observing seasons. Moreover, the system exhibits a high level of chromospheric activity associated with the K1 IV primary component, as demonstrated by strong chromospheric emission in the Mg II h & k, Ca II H & K, H_{α} , and Ca II IRT lines (Jakate et al. 1976; Bopp 1981; Ramsey & Nations 1981; Huenemoerder & Ramsey 1984; Fernández et al. 1986; Popper 1988; Frasca & Catalano 1994; Kang et al. 2003; Eaton & Henry 2007; Zhang & Gu 2008; Cao & Gu 2012). Zhang & Gu (2008) analyzed several chromospheric activity indicators Ca II IRT, H_{α} , Na I D₁, D₂ doublet, and He I D₃ lines by using the spectral subtraction technique and found that the chromospheric activity emissions of the Ca II $\lambda 8542$, $\lambda 8662$, and H_{α} lines are more strong near the two quadratures of the system.

The very unusual behavior of the H_{α} line of SZ Psc has been reported several times. For example, Bopp (1981) detected a remarkable H_{α} outburst in 1978, with the line profile evolving from weak absorption to a broad double-peaked emission during a few nights, and attributed this change to a transient mass-transfer event. In 1979, another H_{α} eruption event was observed by Ramsey & Nations (1981) and interpreted as an intense flare-like event. Huenemoerder & Ramsey (1984) also found a large H_{α} outburst during and after which the profiles suggest a circumstellar origin. Moreover, excess absorption features in the subtracted H_{α} profiles caused by prominence-like material have been discussed by Zhang & Gu (2008) and Cao & Gu (2012).

X-ray emission from the SZ Psc system was first detected by Walter & Bowyer (1981) using the *Einstein Observatory* IPC, demonstrating that RS CVn systems as a class are producers of copious soft X-ray emission. X-ray variability is quite common in such systems (Fuhrmeister & Schmitt 2003) and a strong X-ray flare-like event on the SZ Psc system was detected by the Gas Slit

Camera (GSC) of the Monitor of All-sky X-ray Image (MAXI) on 2011 November 5 (Negoro et al. 2011), which lasted for about five hours; we note that the occurrence of this event was very close to our observing run. Also, the X-ray luminosity of this flare-like event was two times larger than the previous one observed by the MAXI/GSC on 2009 December 4 (also see Negoro et al. 2011).

In summary, SZ Psc is a notable star showing strong magnetic activity with very variable activity features. In this paper, we present the results of our time-resolved spectroscopic observations and simultaneous analysis of several optical chromospheric activity indicators. In Section 2, we provide the details of our spectroscopic observations and data reduction. The procedure of the spectral analysis and the behavior of chromospheric activity indicators are described in Section 3, and in Section 4, the magnetic activity phenomena observed on SZ Psc are discussed in detail. Finally, we present the conclusions in Section 5.

2 SPECTROSCOPIC OBSERVATIONS AND DATA REDUCTION

The time series of high-resolution spectra of SZ Psc analyzed and discussed in this paper were obtained during two consecutive observing nights on October 24 and 25, 2011. Our observations were carried out with the direct echelle mode (DEM) of the Lijiang Exoplanet Tracker (LiJET) mounted on the 2.4-m telescope (Fan et al. 2015) at the Lijiang station, administered by Yunnan Observatories, Chinese Academy of Sciences. The echelle spectrograph has a resolving power $R = \lambda/\Delta\lambda \simeq 28000$ over the wavelength range from 3900 to 9500 Å, and a 4096×4096 -pixel CCD detector was used to record the spectra.

We provide an observing log of the SZ Psc observations in Table 1, which includes the observing date, UT, the heliocentric Julian date (HJD), the orbital phase, and the exposure time. The orbital phases are calculated using the ephemeris

$$HJD = 2,449,284.4483 + 3^d.96566356 \times E \quad (1)$$

from Eaton & Henry (2007), where the epoch corresponds to the conjunction with the K1 IV star “in front”. Our observations lasted for about 5.7 hours in the first night, while the observations had a duration of about 4.6 hours in the second night. In total, 51 spectra of SZ Psc were obtained, with exposure times of typically 600 seconds and sometimes 900 seconds, providing a high time-resolution sampling for the system with a period of nearly four days. In addition, two inactive stars with spectral types and luminosity classes similar to the components of SZ Psc to be used as templates for our spectral subtraction technique and a fast rotating early-type star to be used as a telluric template were also observed with the same instrumental setup.

The spectral reduction was performed with the IRAF¹ package following the standard procedures (image trimming,

¹ IRAF is distributed by the National Optical Astronomy Observatories, which is operated by the Association of Universities for Research in Astronomy (AURA), Inc., under cooperative agreement with the National Science Foundation (NSF).

Table 1. Observing log of SZ Psc.

UT (hh:mm:ss)	HJD (2,455,000+)	Phase	Exp.time (s)
October 24, 2011			
12:32:22	859.0269	0.8760	600
12:51:43	859.0403	0.8794	900
13:09:34	859.0527	0.8825	900
13:26:36	859.0645	0.8855	900
13:43:35	859.0763	0.8885	900
14:00:50	859.0883	0.8915	900
14:15:31	859.0985	0.8941	600
14:27:36	859.1069	0.8962	600
14:39:36	859.1152	0.8983	600
14:51:37	859.1236	0.9004	600
15:03:40	859.1319	0.9025	600
15:15:42	859.1403	0.9046	600
15:27:51	859.1487	0.9068	600
15:39:55	859.1571	0.9089	600
15:51:58	859.1655	0.9110	600
16:04:01	859.1738	0.9131	600
16:16:02	859.1822	0.9152	600
16:28:03	859.1905	0.9173	600
16:40:05	859.1989	0.9194	600
16:52:08	859.2073	0.9215	600
17:04:09	859.2156	0.9236	600
17:16:18	859.2240	0.9258	600
17:28:26	859.2325	0.9279	600
17:40:30	859.2408	0.9300	600
17:52:35	859.2492	0.9321	600
18:04:36	859.2576	0.9342	600
18:16:40	859.2660	0.9363	600
October 25, 2011			
13:56:25	860.0852	0.1429	600
14:08:37	860.0936	0.1450	600
14:20:44	860.1020	0.1472	600
14:32:44	860.1104	0.1493	600
14:44:43	860.1187	0.1514	600
14:56:46	860.1271	0.1535	600
15:08:47	860.1354	0.1556	600
15:20:49	860.1439	0.1577	600
15:32:50	860.1521	0.1598	600
15:44:53	860.1605	0.1619	600
15:56:54	860.1688	0.1640	600
16:08:54	860.1772	0.1661	600
16:20:57	860.1855	0.1682	600
16:33:01	860.1939	0.1703	600
16:45:05	860.2023	0.1724	600
16:57:09	860.2107	0.1745	600
17:09:11	860.2190	0.1767	600
17:21:14	860.2274	0.1788	600
17:33:24	860.2358	0.1809	600
17:45:27	860.2442	0.1830	600
17:57:45	860.2528	0.1852	600
18:10:01	860.2613	0.1873	600
18:22:02	860.2696	0.1894	600
18:34:03	860.2780	0.1915	600

bias correction, scattered light subtraction, 1-D spectrum extraction, wavelength calibration, flat-field division, and continuum fitting). The wavelength calibration was obtained by using the emission lines of a Th-Ar lamp, and the flat-field division was performed by using the high signal-to-noise ratio (SNR) spectrum of the rapidly rotating early-type star

HR 7894 (B5 IV, $v \sin i = 330 \text{ km s}^{-1}$). The spectrum of early-type star was normalized along the line profiles to provide not only a valuable flat-field template, but also was used to remove telluric absorption lines in the chromospheric activity line regions of interest with an interactive procedure in IRAF. Examples of removing the telluric lines in different spectral regions can be found in Gu et al. (2002).

To compare the behavior of chromospheric activity indicators between our two observing nights in detail, we show some examples of the normalized Ca II $\lambda 8542$, $\lambda 8498$, H_{α} , Na I D₁, D₂ doublet, He I D₃, Mg I b triplet, and H_{β} line profiles for each night in Fig. 1. The observing time and orbital phases are also marked in the figure.

3 ANALYSIS OF CHROMOSPHERIC ACTIVITY INDICATORS

The wide wavelength coverage of our echelle spectra allows us to simultaneously study the behavior of all the optical chromospheric activity indicators formed at different atmospheric heights from the region of temperature minimum to the upper chromosphere, including the Ca II IRT ($\lambda 8662$, $\lambda 8542$ and $\lambda 8498$), H_{α} , H_{β} , Ca II H & K, Na I D₁, D₂ doublet, Mg I b triplet ($\lambda 5183$, $\lambda 5172$ and $\lambda 5167$), and He I D₃ lines. Because the SNR is very low in the Ca II H & K line regions and the Ca II $\lambda 8662$ line is located at the very edge of the echelle frame, these three lines are not analyzed in the present paper.

3.1 Spectral subtraction

To extract the spectroscopic signatures caused by stellar activity from the observed spectrum, we apply the spectral subtraction technique to all observed spectra with the help of the program STARMOD (Barden 1985; Montes et al. 1995a,b, 1997, 2000). This subtraction technique has been widely used for chromospheric activity studies (e.g. Montes et al. 1995b, 1997, 2000; Gu et al. 2002; Frasca et al. 2008; Zhang & Gu 2008; Cao & Gu 2014, 2015, 2017; Zhang et al. 2016) and has also been applied for the detection of stellar prominences (Hall & Ramsey 1992; Gunn & Doyle 1997; Gunn, Doyle, & Houdebine 1997; Cao & Gu 2012).

Although a spectral line from the third star has been found in the SZ Psc spectrum, this third light contribution is very weak. Thus, spectra of two inactive stars, HR 7690 (K1 IV) and HR 7560 (F8 V), are respectively used as templates for the primary and secondary component of the system to construct the synthesized spectra representing the non-active state of SZ Psc. The rotational velocity ($v \sin(i)$) value of each component of the SZ Psc system is determined from our template spectra. Using the STARMOD program, we obtain the average $v \sin(i)$ values of 78 km s^{-1} for the primary and 2 km s^{-1} for the secondary, using the high SNR spectra, spanning the wavelength regions 5920–6470 Å which contain many photospheric absorption lines. Our derived values are fully consistent with the results of 80 & 5 km s^{-1} measured with different reference spectra by Eaton & Henry (2007), 78 & 0 km s^{-1} by Zhang & Gu

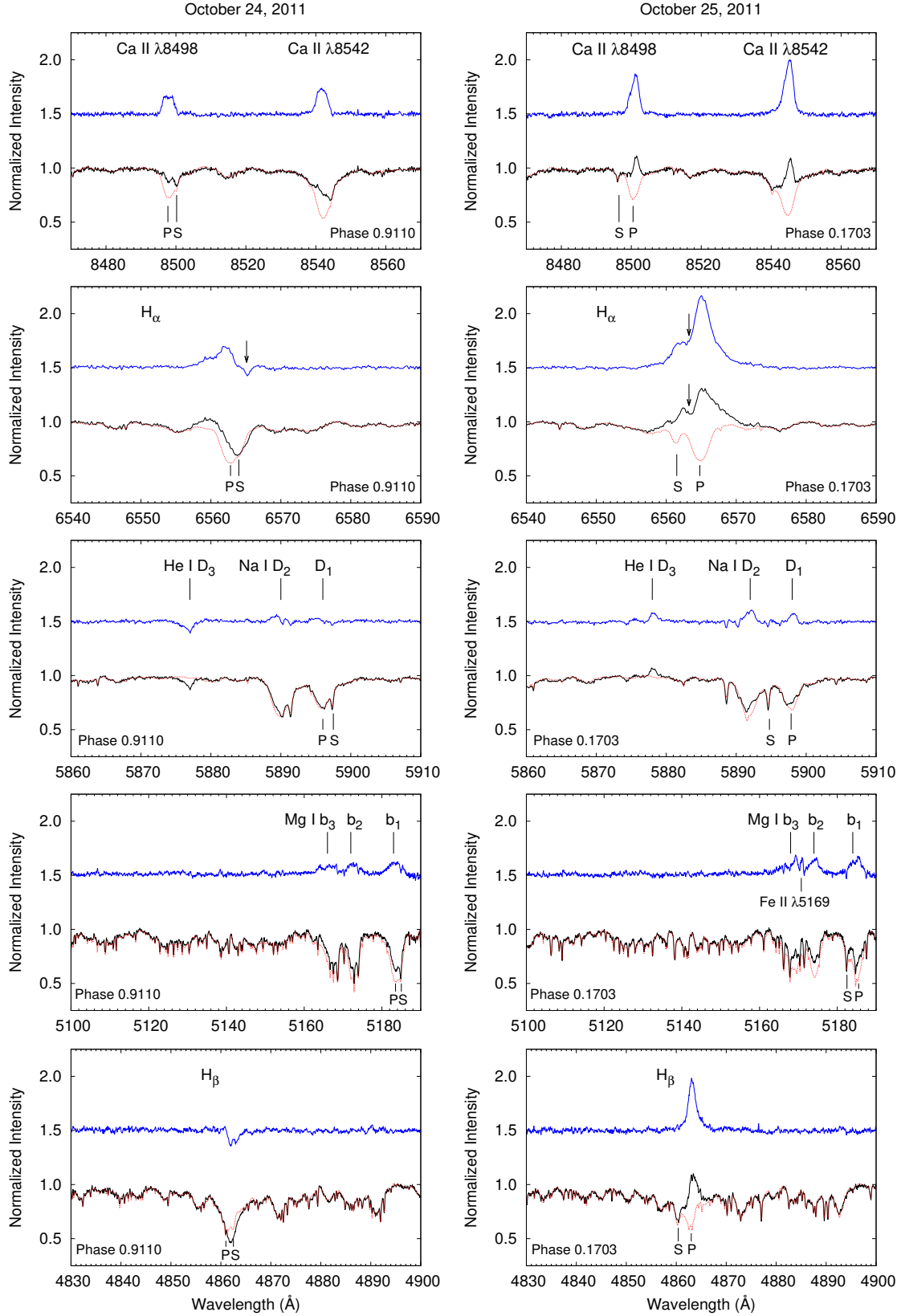


Figure 1. Examples of the observed, synthesized, and subtracted spectra for the Ca II $\lambda 8542$ and $\lambda 8498$, H_{α} , Na I D_1 , D_2 doublet, He I D_3 , Mg I b triplet, and H_{β} line spectral regions. Left panels are examples of our observations on October 24, while right panels show examples of October 25. For each panel, the lower solid-line is the observed spectrum, the dotted line represents the synthesized spectrum and the upper solid line is the subtracted one, shifted for better display. “P” and “S” indicate the primary and secondary components of the SZ Psc system, respectively. Arrows indicate the absorption features presented in the line profiles.

(2008), and $76.9 \text{ \& } 3.4 \text{ km s}^{-1}$ by Cao & Gu (2012). Moreover, the adopted intensity weight ratios are 0.83/0.17 for the Ca II $\lambda 8542, \lambda 8498$ spectral region, 0.815/0.185 for the H α spectral region, 0.775/0.225 for the Na I D_{1, 2} doublet and He I D₃ spectral region, 0.725/0.275 for the Mg I b triplet spectral region, and 0.70/0.30 for the H β spectral region. Consequently, the synthesized spectra in all the observing phases are constructed by properly broadening and weighting the reference spectra to the values of $v \sin(i)$ and the intensity weight ratios derived above, and shifting along the radial velocity axis. Finally, the subtracted spectra between the observed and the synthesized spectra are derived for SZ Psc, which present activity contribution as excess emission or absorption features above or below the continuum level. We present some examples of our spectral subtraction in the Ca II $\lambda 8542, \lambda 8498$, H α , Na I D_{1, 2} doublet, He I D₃, Mg I b triplet, and H β line regions in Fig. 1.

3.2 The behavior of chromospheric activity indicators

After applying the spectral subtraction technique as shown in Fig. 1, it becomes clear the excess emission is associated with the primary K1 IV component of the system, which dominates the activity in the SZ Psc system. The equivalent widths (EWs) of the subtracted Ca II $\lambda 8542, \lambda 8498$, H α , Na I D_{1, 2} doublet, He I D₃, and H β line profiles are measured with the *splot* task in IRAF, using the same method described in our previous papers (Cao & Gu 2015), and are summarized in Table 2 together with their errors; we also provide the ratios of the excess emission $\text{EW}(\lambda 8542)/\text{EW}(\lambda 8498)$, and the $E_{H\alpha}/E_{H\beta}$ values for the observations on October 25, which are calculated from the excess emission $\text{EW}(H\alpha)/\text{EW}(H\beta)$ ratios assuming that the continuum at H α and H β line regions have a flux ratio appropriate to a blackbody (see the detailed description in Section 4.2). We plot the EWs of the subtraction profiles as a function of orbital phase in Fig. 2, which shows that the level of activity is much higher in the second observing night; for example, the EWs of the subtracted H α emission are about 3.5 ~ 5 times stronger on October 25 than the previous night, while the EWs of the Ca II $\lambda 8542$ and $\lambda 8498$ lines are about 1.5 ~ 2 times larger.

The $\text{EW}(\lambda 8542)/\text{EW}(\lambda 8498)$ values are obtained around ~ 1.4 in the first observing night, which are somewhat smaller than the values around ~ 1.6 derived in the second night, when a strong optical flare decay was detected (also see the Section 4.2). These low ratios are consistent with the values found for several other stars with strong chromospheric activity (e.g. Montes et al. 2000; Gu et al. 2002; López-Santiago et al. 2003; Zhang & Gu 2008; Gálvez et al. 2009; Cao & Gu 2014, 2015, 2017; Zhang et al. 2016), which suggests that the Ca II IRT line emission arises from plage-like regions. The $E_{H\alpha}/E_{H\beta}$ ratios have also been usually used as a diagnostic for discriminating the presence of different structures on the stellar surface. As Huenemoerder & Ramsey (1987) discussed, the low ratios in RS CVn-type stars are caused by plage-like regions, while prominence-like structures have high values. Similar results have also been reported by Hall & Ramsey (1992) who found that low ratios ($\sim 1-2$) can be achieved both in plages and

prominences viewed against the disk, but high values ($\sim 3-15$) can only be obtained in extended prominence-like structures viewed off the stellar limb. We obtain the ratios on SZ Psc during the flare decay phase change from 2.40 to 3.40, which are not especially high and anti-correlated with the variation of activity emission shown in Fig. 3, in which the EWs of H α and H β line subtraction and the $E_{H\alpha}/E_{H\beta}$ values are plotted as a function of orbital phase. Especially when the EWs have an increasing oscillation during the gradually decrease, which is resulted from flare ejection (see the discussion in Section 4.2), the ratios have a similar anti-correlation feature. These facts suggest that the low $E_{H\alpha}/E_{H\beta}$ ratios and its variation might be dominantly associated with the flare decrease, and accompanied cool post-flare loops (see the Section 4.3) might play a part of role for the low ratios, which may have a state like absorbing prominence projected against the disk.

The chromospheric activity indicators Ca II $\lambda 8542, \lambda 8498$, H α , Na I D_{1, 2} doublet, He I D₃, Mg I b triplet, and H β lines are characterized by deep absorption features in the observations on October 24. The subtracted H α line shows obvious excess emission above the continuum level, but there is a local absorption feature appearing in the red wing of the subtracted profile (as indicated by the arrow in Fig. 1). The H β line also exhibits an excess absorption in comparison to the inactive synthesized spectrum. An absorption feature also appears around the He I D₃ line region in both observed and subtracted spectra. Moreover, similar absorption signatures are also detected in the other chromospheric activity indicators and the excess absorption features are very evident in the H α , H β and He I D₃ lines. To further analyze the behavior of the excess absorption in our time series shown in Fig. 4, we correct the subtracted line profiles to the rest frame of the primary star in the SZ Psc system, and find that the velocity of the excess absorption features are gradually blue-shifted relative to the primary component and the intensity of the absorption strengthened with time during our observations.

In the observations on October 25, the Ca II $\lambda 8542, \lambda 8498$, H α , He I D₃ and H β lines show strong emission features, which are remarkably different from our observations in the previous night. For the H α line, an obvious absorption feature appears in the blue wing of the strong emission profile (as indicated by the arrow in Fig. 1). Spectral subtraction shows that this absorption resulted in a strong depression in the blue wing of the subtracted emission profile. To clearly see the evolution of the line profile, we correct the observed and subtracted H α spectra to the rest frame of the primary component along the velocity axis in Fig. 5. Similar absorption features could also be found in the H β line, but they are much weaker than in the H α line. The usual chromospheric flare diagnostic He I D₃ line exhibits obvious emission above the continuum level, implying that a strong optical flare event took place on SZ Psc. For the Ca II $\lambda 8542, \lambda 8498$ lines, the strong subtracted emission profiles are asymmetric due to the absorption feature appearing in the blue wing. Comparing with the behavior of the Na I D_{1, 2} doublet and Mg I b triplet lines obtained in the previous night, a strong fill-in of chromospheric emission from the primary component was observed in the subtracted spectra.

Table 2. Measurements for the subtraction profiles of the Ca II $\lambda 8542$, $\lambda 8498$, H α , Na I D₁, D₂ doublet, He I D₃ and H β lines, and ratios of EW($\lambda 8542$)/EW($\lambda 8498$) and E_{H α }/E_{H β }/.}}

Phase	EW(Å)						EW($\lambda 8542$)	E _{Hα}/}	
	Ca II $\lambda 8542$	Ca II $\lambda 8498$	H α	Na I D ₁	Na I D ₂	He I D ₃	EW($\lambda 8498$)	E _{Hβ}/}	
October 24, 2011									
0.8760	0.853±0.013	0.598±0.009	0.711±0.011	-0.159±0.009	-0.250±0.005	1.43	...
0.8794	0.854±0.012	0.585±0.010	0.664±0.005	-0.159±0.011	-0.255±0.015	1.46	...
0.8825	0.821±0.005	0.587±0.005	0.655±0.020	-0.163±0.007	-0.265±0.007	1.40	...
0.8855	0.861±0.008	0.591±0.015	0.675±0.004	-0.159±0.009	-0.263±0.009	1.46	...
0.8885	0.794±0.003	0.584±0.005	0.661±0.006	-0.161±0.011	-0.272±0.012	1.36	...
0.8915	0.823±0.005	0.586±0.006	0.633±0.002	-0.162±0.005	-0.273±0.011	1.40	...
0.8941	0.817±0.014	0.579±0.010	0.622±0.005	-0.160±0.009	-0.270±0.006	1.41	...
0.8962	0.858±0.023	0.584±0.005	0.620±0.010	-0.162±0.006	-0.271±0.012	1.47	...
0.8983	0.844±0.013	0.591±0.007	0.566±0.005	-0.164±0.011	-0.271±0.010	1.43	...
0.9004	0.845±0.005	0.582±0.003	0.560±0.010	-0.166±0.010	-0.280±0.011	1.45	...
0.9025	0.804±0.014	0.588±0.006	0.584±0.006	-0.166±0.008	-0.282±0.009	1.37	...
0.9046	0.824±0.005	0.590±0.005	0.582±0.003	-0.168±0.011	-0.284±0.013	1.40	...
0.9068	0.817±0.013	0.575±0.006	0.576±0.005	-0.169±0.010	-0.291±0.012	1.42	...
0.9089	0.820±0.017	0.604±0.005	0.620±0.019	-0.167±0.012	-0.293±0.009	1.36	...
0.9110	0.843±0.007	0.594±0.005	0.614±0.011	-0.163±0.011	-0.300±0.013	1.42	...
0.9131	0.870±0.013	0.597±0.006	0.574±0.012	-0.168±0.015	-0.297±0.006	1.46	...
0.9152	0.810±0.010	0.582±0.008	0.595±0.004	-0.170±0.013	-0.298±0.007	1.39	...
0.9173	0.815±0.006	0.586±0.003	0.602±0.006	-0.171±0.012	-0.306±0.010	1.39	...
0.9194	0.860±0.004	0.585±0.007	0.584±0.010	-0.173±0.010	-0.305±0.009	1.47	...
0.9215	0.858±0.015	0.595±0.004	0.584±0.006	-0.176±0.011	-0.303±0.011	1.44	...
0.9236	0.870±0.011	0.580±0.005	0.586±0.003	-0.174±0.009	-0.304±0.014	1.50	...
0.9258	0.867±0.017	0.590±0.005	0.577±0.013	-0.172±0.013	-0.304±0.009	1.47	...
0.9279	0.860±0.010	0.583±0.002	0.595±0.002	-0.175±0.011	-0.305±0.011	1.48	...
0.9300	0.865±0.003	0.610±0.010	0.597±0.007	-0.175±0.007	-0.302±0.013	1.42	...
0.9321	0.860±0.004	0.595±0.007	0.585±0.010	-0.178±0.010	-0.305±0.010	1.45	...
0.9342	0.905±0.014	0.625±0.005	0.582±0.014	-0.174±0.009	-0.298±0.009	1.45	...
0.9363	0.878±0.009	0.620±0.011	0.585±0.003	-0.177±0.005	-0.301±0.011	1.42	...
October 25, 2011									
0.1429	1.648±0.009	0.999±0.012	3.028±0.015	0.095±0.011	0.159±0.009	0.135±0.007	1.154±0.005	1.65	2.40
0.1450	1.623±0.015	1.010±0.008	3.026±0.010	0.092±0.005	0.159±0.011	0.134±0.011	1.113±0.015	1.61	2.49
0.1472	1.664±0.010	1.024±0.011	3.017±0.005	0.090±0.007	0.156±0.013	0.128±0.012	1.083±0.017	1.63	2.55
0.1493	1.649±0.011	1.000±0.004	2.967±0.015	0.090±0.011	0.153±0.010	0.134±0.006	1.109±0.013	1.65	2.45
0.1514	1.639±0.012	1.005±0.008	2.947±0.014	0.095±0.010	0.156±0.009	0.130±0.005	1.062±0.002	1.63	2.54
0.1535	1.611±0.008	0.993±0.004	2.933±0.011	0.083±0.009	0.151±0.011	0.120±0.009	1.015±0.013	1.62	2.65
0.1556	1.602±0.013	1.008±0.009	2.864±0.010	0.084±0.013	0.157±0.012	0.118±0.013	1.015±0.006	1.59	2.58
0.1577	1.604±0.007	0.957±0.007	2.860±0.011	0.087±0.012	0.159±0.010	0.112±0.011	1.005±0.017	1.68	2.61
0.1598	1.646±0.005	1.001±0.007	2.838±0.010	0.080±0.010	0.151±0.009	0.106±0.010	0.951±0.019	1.64	2.73
0.1619	1.643±0.009	0.987±0.003	2.774±0.020	0.083±0.009	0.154±0.005	0.103±0.008	0.946±0.013	1.66	2.69
0.1640	1.634±0.011	0.996±0.004	2.770±0.015	0.082±0.007	0.158±0.007	0.111±0.011	0.912±0.006	1.64	2.78
0.1661	1.679±0.010	0.992±0.005	2.908±0.016	0.076±0.011	0.151±0.011	0.098±0.015	0.988±0.005	1.69	2.70
0.1682	1.649±0.012	0.997±0.007	2.955±0.009	0.081±0.010	0.152±0.012	0.104±0.013	1.024±0.010	1.65	2.64
0.1703	1.645±0.007	1.003±0.003	3.007±0.014	0.078±0.008	0.150±0.010	0.097±0.007	1.058±0.005	1.64	2.60
0.1724	1.636±0.009	1.001±0.008	2.991±0.011	0.083±0.009	0.146±0.008	0.106±0.009	0.998±0.010	1.63	2.75
0.1745	1.599±0.007	1.028±0.013	2.880±0.015	0.072±0.007	0.145±0.005	0.092±0.005	0.978±0.003	1.56	2.70
0.1767	1.662±0.011	1.029±0.011	2.815±0.008	0.079±0.010	0.145±0.013	0.087±0.008	0.953±0.006	1.62	2.71
0.1788	1.646±0.013	0.998±0.006	2.766±0.011	0.085±0.008	0.146±0.006	0.090±0.010	0.907±0.014	1.65	2.79
0.1809	1.678±0.009	0.987±0.005	2.732±0.012	0.079±0.011	0.149±0.009	0.086±0.013	0.887±0.013	1.70	2.82
0.1830	1.624±0.006	1.000±0.003	2.693±0.010	0.082±0.012	0.146±0.010	0.088±0.012	0.848±0.015	1.62	2.91
0.1852	1.572±0.008	0.990±0.004	2.623±0.010	0.075±0.010	0.148±0.008	0.080±0.011	0.792±0.012	1.59	3.03
0.1873	1.608±0.010	0.991±0.007	2.740±0.013	0.077±0.007	0.149±0.011	0.086±0.010	0.783±0.007	1.62	3.21
0.1894	1.637±0.005	0.982±0.009	2.569±0.015	0.079±0.009	0.143±0.012	0.078±0.012	0.723±0.005	1.67	3.25
0.1915	1.613±0.007	0.976±0.006	2.537±0.010	0.076±0.005	0.141±0.013	0.074±0.006	0.683±0.012	1.65	3.40

Note: Negative EWs indicate that the subtraction profiles characterized by absorption features.

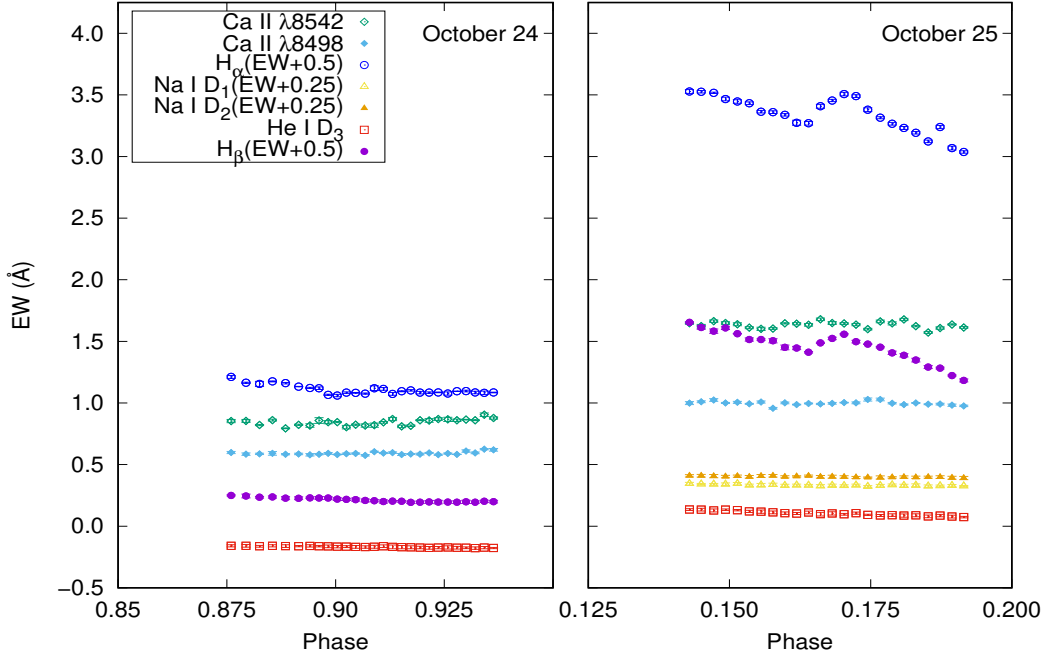


Figure 2. EWs of the subtracted Ca II $\lambda 8542$, $\lambda 8498$, H_{α} , Na I D₁, D₂ doublet, He I D₃ and H_{β} lines versus orbital phase during our two night observations. For better visibility, we shift EWs of the H_{α} , Na I D₁, D₂ doublet, and H_{β} lines through adding offsets. The label identifying each optical chromospheric activity indicator is marked in the plot, and offset values are also given in the label.

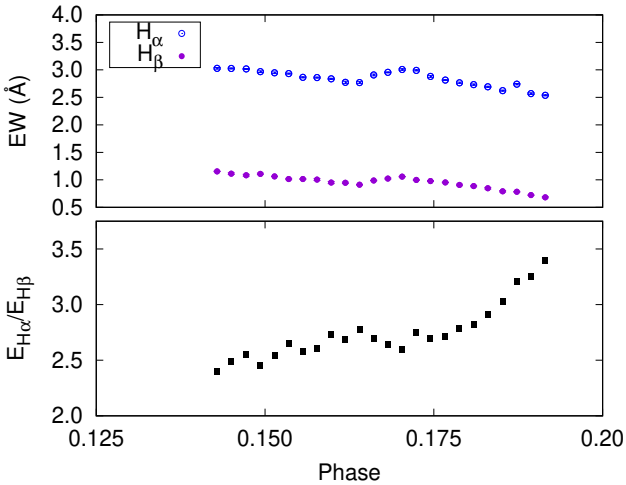


Figure 3. Comparison between the $E_{H_{\alpha}}/E_{H_{\beta}}$ ratios and the chromospheric emission variations in H_{α} and H_{β} lines.

4 DISCUSSION

4.1 Prominence activation

In the observations on October 24, the He I D₃ line shows an absorption feature and, further, there is unusual excess absorption appearing in the subtracted H_{α} , H_{β} and other lines. We interpret the absorption features as caused by a prominence while being seen in projection against a significant fraction of the stellar disk. Stellar prominences have been reported for the first time by Robinson & Collier Cameron (1986) as transient absorption features passing through the rotationally broadened H_{α}

profile of the rapidly rotating K0 dwarf star AB Dor. The absorption features are thought to originate in cool clouds of mostly neutral material magnetically supported high above the stellar photosphere and forced to corotate with the star in a manner of reminiscent of solar quiescent prominences, which scatter the underlying chromospheric emission out of the line-of-sight as they transit the stellar disc (Collier Cameron & Robinson 1989a,b). Stellar prominences with heights of several stellar radii lying at or beyond the corotation radius of the star have lifetimes on the order of one week (Collier Cameron & Robinson 1989a,b). Similar quiescent stellar prominence characteristics have now been detected on several rapidly rotating single active stars, such as AB Dor (Collier Cameron & Robinson 1989a,b), G dwarfs in the α Per cluster (Collier Cameron & Woods 1992), BO Mic (Jeffries 1993; Dunstone et al. 2006; Wolter et al. 2008), HK Aqr (Byrne, Eibe, & Rolleston 1996), PZ Tel (Barnes et al. 2000), RX J1508.6-4423 (Donati et al. 2000) and RE 1816+514 (Eibe 1998). Moreover, Hall & Ramsey (1992) also found prominence-like hints in eight of ten RS CVn-type systems studied during their survey and concluded that stellar prominences may be common phenomena in this type stars.

Because the primary is very active in the SZ Psc system, we infer that prominence is associated with this star. Although the absorption features appear very near the velocity of the secondary (see Fig. 1), moreover, it is uncertain whether prominence is obscuring the part of the secondary. If this situation happened, the absorption features caused by prominence which is associated with the primary would have redward motion relative to the velocity of the secondary due to the orbital motion of the system during our observations. But the fact is that there

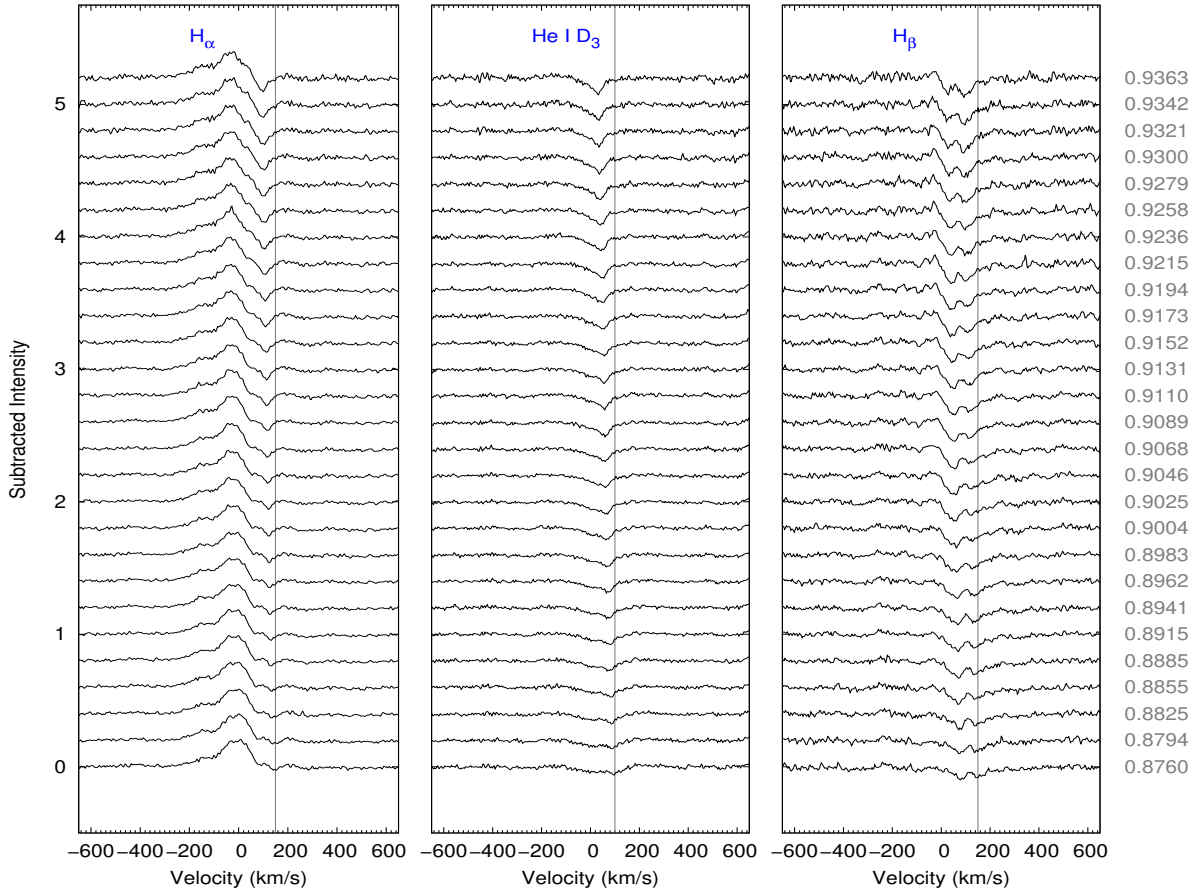


Figure 4. Series of the subtracted H_{α} , He I D_3 and H_{β} line profiles obtained during the observations on October 24, and corrected to the rest velocity frame of the primary component of the SZ Psc system. Spectra are shifted arbitrarily for better visibility. The vertical lines highlight the motion of absorption features and the phases are also marked in the plot.

is no obvious shift for the absorption features when we correct the subtracted line profiles to the rest frame of the secondary, unless prominence has motion of its own which result in the absorption shift and just exactly offset the redward motion. However, taking into account the line profile of the primary is very broad and thus it is more possible the absorption features are resulted from prominence which is absorbing the emission and continuum of the red wing from the primary, especially at the end of the observations on October 24 in the H_{α} line, we tend to think that prominence is obscuring the part of the primary.

According to the gradual blue-shift of the absorption relative to the underlying spectrum of the primary star and the increasing strength, this absorption could be understood in terms of an accelerated upward motion of the prominence material. As observed for the Sun, preceding the onset of a large (typically two-ribbon) flare, there might be transient signatures of flare-related activity occurring in the activity region itself or its neighborhood. It is widely accepted that prominence (filament) activation is closely tied to two-ribbon flares (Ding et al. 2003; Sterling & Moore 2005; Chifor et al. 2007). Prior to the flare, a prominence (filament), located at the neutral lines of a two-ribbon flare, will become unstable due to some magnetic processes (e.g. Mikic & Linker 1994; Forbes & Priest 1995;

Chen & Shibata 2000), appearing as a rising motion or even an eruption. For our observations, there is a strong optical flare event in the second observing night (see Section 4.2). More importantly, both the excess absorption event and the optical flare observed during two consecutive nights may have occurred at the same hemisphere for a nearly four days periodic system, and therefore we think it is possible that both of them arise from the related active region. Furthermore, as discussed in next section, a X-ray flare-like event was detected at the same hemisphere after three orbital cycles and around the phase near our observations, indicating that there might be a strong activity region in this hemisphere and all of these activity phenomena are possibly associated with this region. In analogy to the activity phenomena observed in the solar case, we are led to infer that the excess absorption features would be produced due to a prominence activation event rising in height before the eruption of a strong optical flare.

We measure the radial velocities of the excess absorption features relative to the primary component of the system in the chromospheric activity indicators H_{α} , Na I D_2 , He I D_3 and H_{β} lines in the observations on October 24, and plot them against the observing time in Fig. 6. The measured radial velocities are very different in these chromospheric lines, probably due to the fact that

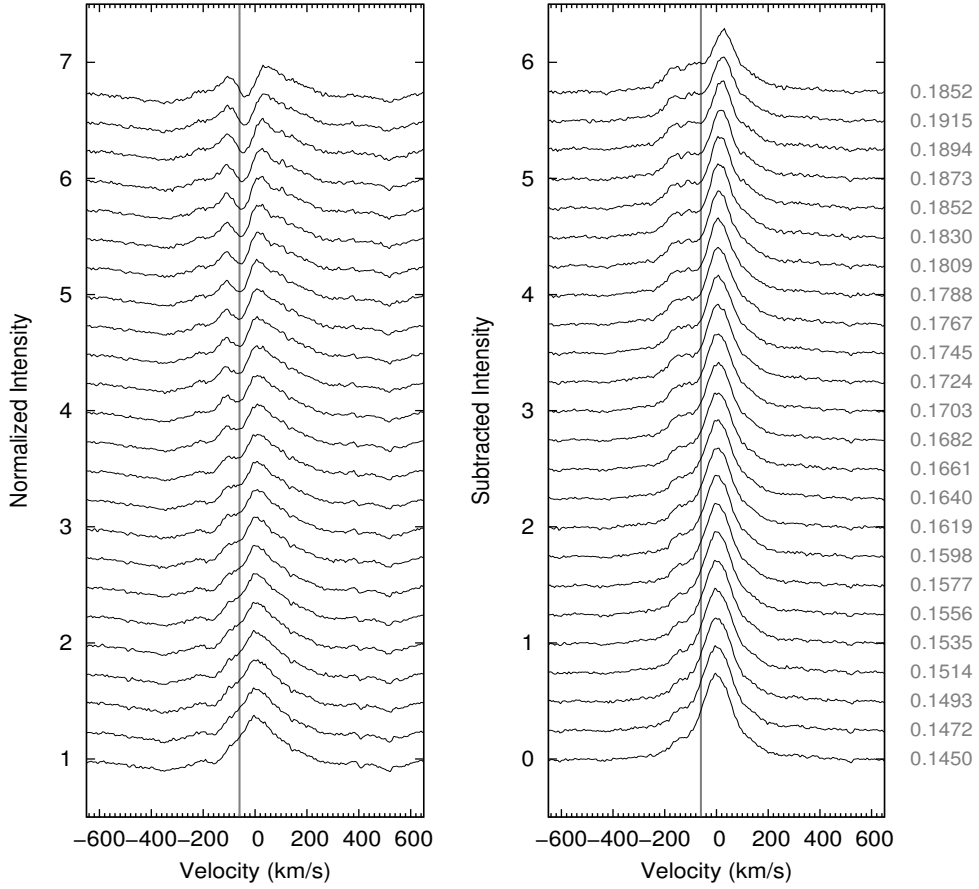


Figure 5. Same as Fig. 4, but for the observed (left panel) and subtracted (right panel) H_α line profiles obtained during the observations on October 25.

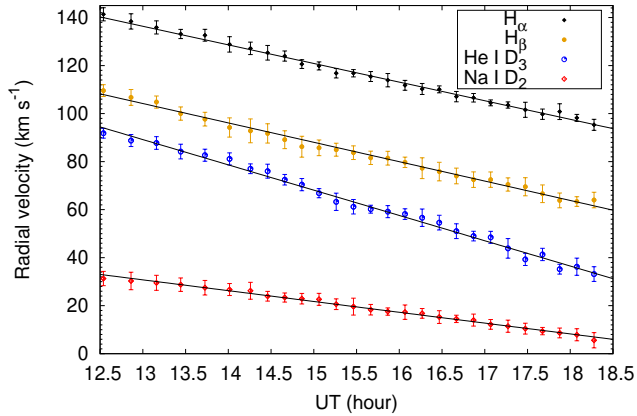


Figure 6. Radial velocities of excess absorption relative to the primary component of the system in the H_α , $Na\ I\ D_2$, $He\ I\ D_3$ and H_β lines during the observations on October 24. Solid lines represent the linear fits, and the label identifying each line is also marked in the plot.

they are formed at different atmospheric heights, which lets the absorption features more or less linearly drift in RV with different rates. Using the measured drift rates, we can make a rough estimate of the height of the prominence raised

along the line-of-sight during observations on October 24 and find values of $0.4 R_\odot$ for the $Na\ I\ D_2$ line formed at the upper photosphere and lower chromosphere, $0.6 R_\odot$ for the H_α and H_β lines formed at the middle chromosphere, and $0.9 R_\odot$ for the $He\ I\ D_3$ line formed at the upper chromosphere.

4.2 Optical flare

Unlike the absorption feature encountered in the previous night, the chromospheric flare indicator $He\ I\ D_3$ line shows obvious emission above the continuum level throughout the observations on October 25, which provides strong support for the occurrence of a large optical flare due to its high excitation potential (Zirin 1988). Moreover, the observed stronger emission in the $Ca\ II\ \lambda 8542$, $\lambda 8498$, H_α and H_β lines also confirms the event as flare activity. Furthermore, as marked in Fig. 1, the $Fe\ II\ \lambda 5169$ line near the $Mg\ I\ b\ \lambda 5167$ line was also found in emission during the flare event, similar to what has also been observed in the young active K2 dwarf stars PW And by López-Santiago et al. (2003) and LQ Hya by Montes et al. (1999).

Stellar flares share many features with solar flares. Solar flares are powerful and explosive phenomena in the outer solar atmosphere, which typically include three ba-

Table 3. Absolute surface fluxes F_S and flare luminosities L released by the chromospheric activity lines.

Line	F_S ($\times 10^7$ erg cm $^{-2}$ s $^{-1}$)	L ($\times 10^{31}$ erg s $^{-1}$)
Ca II λ 8542	0.61	1.32
Ca II λ 8498	0.37	0.81
H α	1.56	3.41
Na I D $_1$	0.06	0.12
Na I D $_2$	0.09	0.20
He I D $_3$	0.08	0.17
H β	0.76	1.65

sic phases during their evolution: the fast rise of the emission intensity, the maximum, and the gradual decay phase (Schrijver & Zwaan 2000). For SZ Psc, we did not capture the whole flare evolution from the initial outburst to the very end due to limited observations and the observing gap between our two observing nights. The overall trend of the flare intensity shows a decrease (see Table 2 and Fig. 2), especially for the H α and H β lines, which suggests that our observation was part of the gradual decay phase of a flare and that the onset of this flare likely occurred around the gap between our two observing nights. Assuming that the first observation (at phase 0.1429) of October 25 corresponds to the flare maximum, we can derive a lower limit to the flare energy. We compute the stellar continuum flux $F_{H\alpha}$ (erg cm $^{-2}$ s $^{-1}$ \AA^{-1}) in the H α line region as a function of the color index $B - V$ (~ 0.846 for SZ Psc; Messina 2008) based on the calibration

$$\log F_{H\alpha} = [7.538 - 1.081(B - V)] \pm 0.33$$

$$0.0 \leq B - V \leq 1.4 \quad (2)$$

by Hall (1996), and convert the EWs into the absolute surface fluxes F_S (erg cm $^{-2}$ s $^{-1}$). Following the method adopted by Montes et al. (1999) and García-Alvarez et al. (2003), we obtain the stellar continuum fluxes by using $F_{H\alpha}$ corrected for the flux ratios F_{6563}/F_λ for the other chromospheric activity lines.

The flux ratios were given by assuming a blackbody with contribution of both the primary and secondary component of the SZ Psc system at the effective temperatures $T_{eff} = 4910$ K and $T_{eff} = 6090$ K (Lanza et al. 2001), in which the contribution ratios of two components have been obtained in the spectral subtraction technique. Therefore, the flare energies L (erg s $^{-1}$) in these lines were derived through converting the absolute surface fluxes into luminosities by using the radius $R_* = 6.0 R_\odot$ of the K1 IV primary component (Eaton & Henry 2007). We assumed that the optical flare occurred on the primary star, and also corrected the EWs to the total continuum before converting to absolute surface fluxes. The absolute surface fluxes and luminosities in the chromospheric activity lines at phase 0.1429 are listed in Table 3. The values for the energy released in the H α line are of similar order of magnitude as the strong flares of other very active RS CVn-type stars, such as V711 Tau (García-Alvarez et al. 2003; Cao & Gu 2015), UX Ari (Montes et al. 1996; Gu et al. 2002; Cao & Gu 2017) and HK Lac (Catalano & Frasca 1994).

Moreover, by comparison, we find that the X-ray flare-like event detected by the MAXI/GSC from 18:20 UT

(= MJD 55870.764) to 23:03 UT (= MJD 55870.960) on 2011 November 5 (Negoro et al. 2011) occurred during phases 0.96–0.01, which is comparable to the phase between our two observing nights but three orbital cycles apart. Therefore, we argue that both X-ray flare-like event and our optical flare may have taken place at a same and long-lived active region over the surface of SZ Psc.

Finally, in Fig. 7 we plot some of the observed and subtracted H α spectra selected at six phases to illustrate the evolution of the line profile; it is clear that there is the notable enhancement in the far blue wing of the H α line emission profiles at velocities between -150 and -200 km s $^{-1}$ during our observations (as indicated by the arrow), and therefore an increasing oscillation occurred when the EWs gradually decrease during the flare decay phase (see Fig. 2), similar to the finding derived by Eibe et al. (1999) for the late-type fast rotator BD+22 $^\circ$ 4409. The excess emission was explained by high velocity ejections of hot chromospheric material during the flare event; similar features could also be found in the H β line.

4.3 Post-flare loops

We detected a fast evolved absorption feature in the blue wing of emission profile in the observations on October 25 (especially for the H α line, see Fig. 5) during the gradual decay phase of the flare. It could be explained by cool post-flare loops seen in projection against the bright flare background. Post-flare loops are arcade-like, developed systems, which are usually found during the gradual decay phase of large two-ribbon flares in the Sun and can last for several hours (Sturrock 1968; Kopp & Pneumann 1976; Forbes & Malherbe 1986). Except for prominence activation event detected in our previous night observations, this post-flare loops also suggest our optical flare to be a two-ribbon flare.

As shown in Fig. 5, the velocity of the absorption feature shows no distinct change relative to the primary component of the system in the initial stage, but the strength gradually increases during our observations, it could be understood that the loops were rising their height at a nearly steady velocity of about -60 km s $^{-1}$. Similar absorption feature at velocity -50 km s $^{-1}$ in the H α line profile during the decay of the flare had been observed by Eibe et al. (1999) on BD+22 $^\circ$ 4409 and also attributed to the development of cool dark flare loops that are seen against the flare background. Considering solar studies, the upward motion of the post-flare loops are caused by the systematic ascending of the magnetic reconnection site in the corona (Sturrock 1968; Kopp & Pneumann 1976; Forbes & Malherbe 1986). For our observation, on the other hand, the absorption feature seems to show an obvious shift toward the red direction from phase 0.1809, which possibly suggests that the post-flare loops began to rise with a gradually decreasing velocity, consistent with what one typically observes in the solar case.

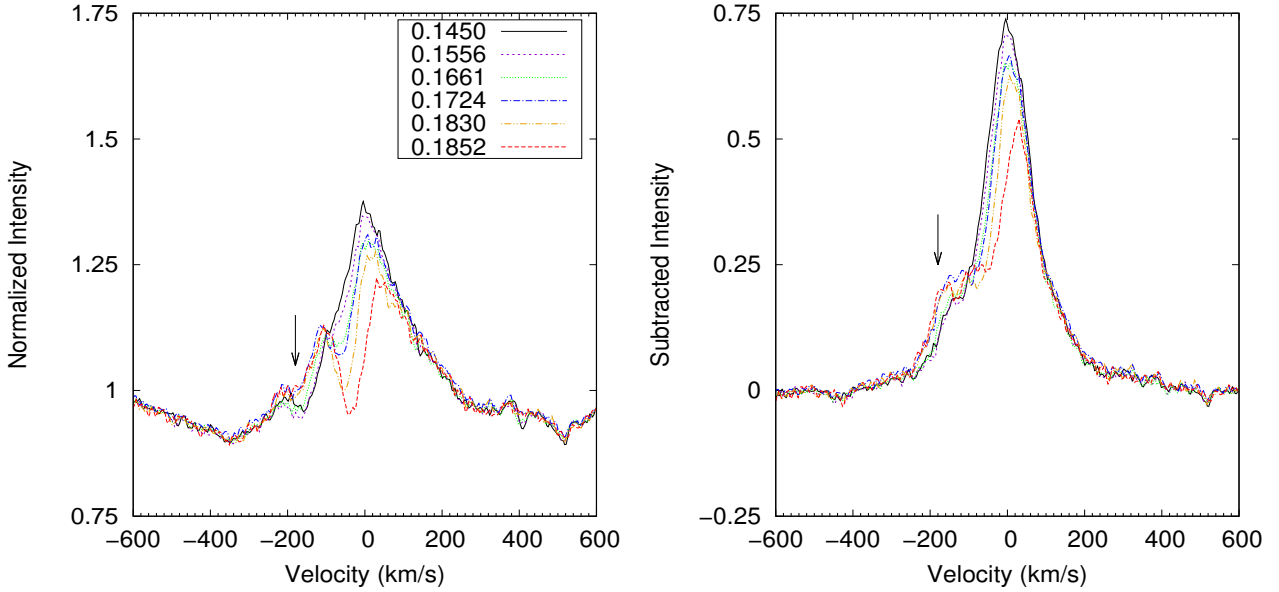


Figure 7. Same as Fig. 5, but for the spectra selected at six phases.

5 CONCLUSIONS

Our analysis of the time-resolved spectroscopic observations of several chromospheric activity indicators (including the Ca II $\lambda 8542$ and $\lambda 8498$, H_{α} , Na I D₁, D₂, He I D₃, Mg I b triplet, and H_{β} lines), taken during two consecutive observing nights on October 24 and 25, 2011, demonstrates the clear detection of a series of magnetic activity phenomena on the very active RS CVn-type star SZ Psc, including a likely prominence activation event, an optical flare, and post-flare loops. The prominence activation occurred on SZ Psc before the occurrence of a strong optical flare was observed in the observations on October 24, and we argue that this prominence event is possibly associated with the subsequent strong optical flare. The gradual decay phase of a large optical flare was detected in the observations on October 25, during which cool post-flare loops were seen as developing absorption features against bright flare background in the chromospheric lines, especially in the H_{α} line. Moreover, the prominence activation event and post-flare loops both indicate that optical flare on SZ Psc can be classified as a two-ribbon flare.

To our knowledge, the detection of such a series of possibly associated magnetic activity phenomena in short period of time is rare in the stellar case. In order to further confirm this series of activity phenomena and investigate the detailed connection among them for the SZ Psc system, we require more high-resolution spectral observations with higher temporal cadence.

ACKNOWLEDGEMENTS

We are hugely grateful to those who contributed to the Li-JET project. We would like to thank all the staff of the 2.4-m telescope of Lijiang station of Yunnan Observatories for their help and support during our observations. Funding for the telescope has been provided by the Chinese

Academy of Sciences (CAS) and the People's Government of Yunnan Province. We acknowledge the support from the Project Based Personnel Exchange Program (PPP) with China Scholarship Council (CSC) and German Academic Exchange Service (DAAD) ([2016] 6041). We also thank the anonymous referee for helpful comments and suggestions, which led to significantly improvement in our manuscript. This work was financially supported by the National Natural Science Foundation of China (NSFC) under grant Nos. 10373023, 10773027 and 11333006, and the CAS through project No. KJCX2-YW-T24, and the CAS "Light of West China" Program.

REFERENCES

- Barden S. C., 1985, *ApJ*, 295, 162
 Barnes J. R., Collier Cameron A., James D. J., Donati J.-F., 2000, *MNRAS*, 314, 162
 Bopp B. W., 1981, *AJ*, 86, 771
 Byrne P. B., Eibe M. T., Rolleston W. R. J., 1996, *A&A*, 311, 651
 Catalano S., Frasca A., 1994, *A&A*, 287, 575
 Cao D. T., Gu S. H., 2012, *A&A*, 538, 130
 Cao D. T., Gu S. H., 2014, *AJ*, 147, 38
 Cao D. T., Gu S. H., 2015, *MNRAS*, 449, 1380
 Cao D. T., Gu S. H., 2017, *Res. Astron. Astrophys.*, 17, 055C
 Chen P. F., Shibata K., 2000, *ApJ*, 545, 524
 Chifor C., Tripathi D., Mason H. E., Dennis B. R., 2007, *A&A*, 472, 967
 Collier Cameron A., Robinson R. D., 1989a, *MNRAS*, 236, 57
 Collier Cameron A., Robinson R. D., 1989b, *MNRAS*, 238, 657
 Collier Cameron A., Woods J. A., 1992, *MNRAS*, 258, 360n
 Ding M. D., Chen Q. R., Li J. P., Chen P. F., 2003, *ApJ*, 598, 683
 Donati J.-F., Mengel M., Carter B. D., Marsden S., Collier Cameron A., Wichmann R., 2000, *MNRAS*, 316, 699
 Dunstone N. J., Barnes J. R., Collier Cameron A., Jardine M., 2006, *MNRAS*, 365, 530
 Eaton J. A., Hall D. S., 1979, *ApJ*, 227, 907
 Eaton J. A., Henry G. W., 2007, *PASP*, 119, 259

- Eibe M. T., 1998, *A&A*, 337, 757
- Eibe M. T., Byrne P. B., Jeffries R. D., Gunn A. G., 1999, *AJ*, 341, 527
- Fan Y. F., Bai J. M., Zhang J. J. et al., 2015, *Res. Astron. Astrophys.*, 15, 918
- Fekel F. C., Moffett T. J., Henry G. W., 1986, *ApJS*, 60, 551
- Fernández-Figueroa M. J., De Castro E., Montesinos B. et al., 1986, *Adv. Space. Res.*, 6, 187
- Forbes T. G., Malherbe J. M., 1986, *ApJ*, 302, L67
- Forbes T. G., Priest E. R., 1995, *ApJ*, 446, 377
- Frasca A., Biazzo K., Taş G., Evren S., Lanzafame A. C., 2008, *A&A*, 479, 557
- Frasca A., Catalano S., 1994, *A&A*, 284, 883
- Fuhrmeister B., & Schmitt J. H. M. M., 2003, *A&A*, 403, 247
- Gálvez M. C., Montes D., Fernández-Figueroa M. J., De Castro E., Cornide M., 2009, *AJ*, 137, 3965
- García-Alvarez D., Foing B. H., Montes D. et al., 2003, *A&A*, 397, 285
- Glazunova L. V., Yushchenko A. V., Tsymbal V. V., Mkrtichian D. E., Lee J. J., Kang Y. W., Valyavin G. G., Lee B.-C., 2008, *AJ*, 136, 1736
- Gu S. H., Tan H. S., Shan H. G., Zhang F. H., 2002, *A&A*, 388, 889
- Gunn A. G., Doyle J. G., 1997, *A&A*, 318, 60
- Gunn A. G., Doyle J. G., Houdebine E. R., 1997, *A&A*, 319, 211
- Hall D. S., 1976, in Fitch W. S., ed, *Multiple Periodic Variable Stars*, IAU Coll. 29. Reidel: Dordrecht, p. 287
- Hall J. C., 1996, *PASP*, 108, 313
- Hall J. C., Ramsey L. W., 1992, *AJ*, 104, 1942
- Huenemoerder D. P., Ramsey L. W., 1984, *AJ*, 89, 549
- Huenemoerder D. P., Ramsey L. W., 1987, *ApJ*, 319, 392
- Jakate S. M., Bakos G. A., Fernie J. D., Heard J. F., 1976, *AJ*, 81, 250
- Jeffries R. D., 1993, *MNRAS*, 262, 369
- Kang Y. W., Lee W.-B., Kim H., Oh K.-D., 2003, *MNRAS*, 344, 1227
- Kopp R. A., Pneumann G. W., 1976, *Sol. Phys.* 50, 85
- Lanza A. F., Rodonò M., Mazzola L., Messina S., 2001, *A&A*, 376, 1011
- López-Santiago J., Montes D., Fernández-Figueroa M. J., Ramsey L. W., 2003, *A&A*, 411, 489
- Messina S., 2008, *A&AS*, 480, 495
- Mikic Z., Linker, J. A., 1994, *ApJ*, 430, 898
- Montes D., Fernández-Figueroa M. J., De Castro E., Cornide M., 1995a, *A&A*, 294, 165
- Montes D., Fernández-Figueroa M. J., De Castro E., Cornide M., 1995b, *A&AS*, 109, 135
- Montes D., Fernández-Figueroa M. J., De Castro E., Cornide M., Latorre A., Sanz-Forcada J., 2000, *A&AS*, 146, 103
- Montes D., Fernández-Figueroa M. J., De Castro E., Sanz-Forcada J., 1997, *A&AS*, 125, 263
- Montes D., Saar S. H., Collier Cameron A., Unruh Y. C., 1999, *MNRAS*, 305, 45
- Montes D., Sanz-Forcada J., Fernández-Figueroa M. J., Lorente R., 1996, *A&A*, 310, L29
- Negoro H., Usui R., Yamazaki K. et al., 2011, *ATel*, 3737
- Popper D. M., 1988, *AJ*, 96, 1040
- Ramsey L. W., Nations H. L., 1981, *PASP*, 93, 732
- Robinson R. D., Collier Cameron A., 1986, *Proc. Astron. Soc. Aust.*, 6, 308
- Schrijver C. J., Zwaan C., 2000, *Solar and stellar magnetic activity*. Cambridge Univ. Press, Cambridge
- Sterling A. C., Moore R. L., 2005, *ApJ*, 630, 1148
- Sturrock P. A., 1968, *IAU Symp.* 35, 471
- Walter F. M., & Bowyer S., 1981, *ApJ*, 245, 671
- Wolter U., Robrade J., Schmitt J. H. M. M., Ness J. U., 2008, *A&A*, 478, L11
- Xiang Y., Gu S. H., Collier Cameron A., Barnes J. R., Zhang L. Y., 2016, *MNRAS*, 456, 314
- Zhang L. Y., Gu S. H., 2008, *A&A*, 487, 709
- Zhang L. Y., Pi Q. F., Han X. M. L., Chang L., Wang D. M., 2016, *MNRAS*, 459, 854
- Zirin H., 1988, *Astrophysics of the Sun*. Cambridge Univ. Press, Cambridge

This paper has been typeset from a $\text{\TeX}/\text{\LaTeX}$ file prepared by the author.